Scientific Research Publishing

Journal of Modern Physics, 2026, 17(2), 124-138
https://www.scirp.org/journal/jmp
ISSN Online: 2153-120X
ISSN Print: 2153-1196

Tunable Single-Photon Nonreciprocal Transmission and Directional Routing in a Microresonator-Waveguide System with Multiple Coupling Points

Jinsong Huang, Le Zhang, Hongwu Huang

School of Information Engineering, Jiangxi University of Science and Technology, Ganzhou, China
Email: jshuangjs@126.com

How to cite this paper: Huang, J.S., Zhang, L. and Huang, H.W. (2026) Tunable Single-Photon Nonreciprocal Transmission and Directional Routing in a Microresonator-Waveguide System with Multiple Coupling Points. *Journal of Modern Physics*, **17**, 124-138.
https://doi.org/10.4236/jmp.2026.172008

Received: January 8, 2026
Accepted: February 9, 2026
Published: February 12, 2026

Abstract

We investigate the controllable single-photon transport via a microresonator coupled to two meandering waveguides at multiple coupling points. Using the analytical expressions of the single-photon scattering amplitudes obtained by the real-space Hamiltonian, the transport characteristics in the waveguide system are demonstrated. These results show that the perfectly nonreciprocal transmission in a single waveguide and the directional routing approaching the unity probability in two waveguides can be achieved by adjusting the resonator-waveguide coupling related to the phase parameter, arising from the phase-dependent interference effect of the multiple point couplings of the resonator. Our proposal may have wide potentials in quantum information processing.

Keywords

Quantum Nonreciprocity, Quantum Routing, Scattering Theory, Optical Waveguide, Microresonator

1. Introduction

The study on manipulating the single-photon transport via the low-dimensional waveguides has motivated great interest due to the potential applications in quantum information processing [1] [2] and quantum networks [3]. In the past decades, waveguide quantum electrodynamic (wQED) [4] [5], which enables strong interactions between quantum emitters and light fields confined in one-dimensional waveguides, provides a powerful platform for realizing controllable single-

photon scattering.

As an indispensable characteristic in the single-photon transmission, nonreciprocal photon transport, which allows the photon to propagate in one direction along a single waveguide but blocks light propagating in the reverse direction, plays an important role in preventing the information backflow in waveguide systems. Consequently, a wide variety of studies on nonreciprocal quantum devices with high contrast ratio have been implemented in various wQED systems, including atomic qubits [6] [7], optical cavities [8] [9], optomechanical or electromechanical systems [10]-[12], and chiral waveguide systems [13] [14]. On the other hand, quantum routing, as another transport characteristic, can transfer quantum information from the input channel to different channels, and has also been demonstrated in numerous wQED systems [15]-[21], where multiple waveguides are utilized as quantum channels, and quantum emitters are used to distribute quantum information. However, in some proposed configurations, the low routing efficiency of no more than 0.5 for the single photons from the input waveguide channel to another may limit more potential applications, and thus it is of considerable interest to design a quantum router with high efficiency.

Optical resonators are useful components for wavelength switching, filtering, and routing applications. Due to their ultra-high quality factor, whispering gallery mode (WGM) optical microresonators have found widespread applications, ranging from sensitive sensing [22], optical switching and routing [23]-[25], coherent non-reciprocity transport [26] [27], and so on. Usually, the microresonator is coupled to a straight waveguide at a single point. Interestingly, a recent report [28] shows that a spinning resonator can interact with a meandering waveguide at multiple coupling points, which results in the complete unidirectional transparency over the whole optical frequency range with no analogy in other quantum devices, due to the interference effects among different coupling points.

In this paper, we study the controllable single-photon transport in a meandering waveguide system coupled with a microresonator. In comparison with the rotary resonator scheme [28], our proposal is simple due to the static implementation without the resonator spinning. By using a real-space approach, the scattering amplitudes of single photons are derived analytically and the transport properties are discussed in detail. Numerical results show that the perfectly nonreciprocal transport and high-efficiency routing of single photons can be implemented via the joint effect of the local coupling phase and the accumulated phase of the photon propagating between two coupling points of the resonator, and the targeted routing efficiency with approximating 100% routing probability can be realized in two output ports owing to the phase-dependent interference effect. The proposed scattering system may be exploited potentially in designing high-efficiency quantum optical devices.

2. Theoretical Model

A schematic view of the composite system is displayed in **Figure 1**, where two

one-dimensional waveguides is linked by a two-mode WGM resonator. The WGM resonator supports two degenerate propagating modes, described separately by the creation operator $c_1^\dagger$ of the clockwise mode and $c_2^\dagger$ of the counterclockwise mode, with the common frequency ω_r and the intrinsic decay rate γ_r. The resonator is coupled to the waveguide $W_{a(b)}$ through two connecting points located at $x=0$ and $x=d_{a(b)}$. When a single photon is injected into the waveguide, it will be scattered to four ports of the two waveguides by the resonator.

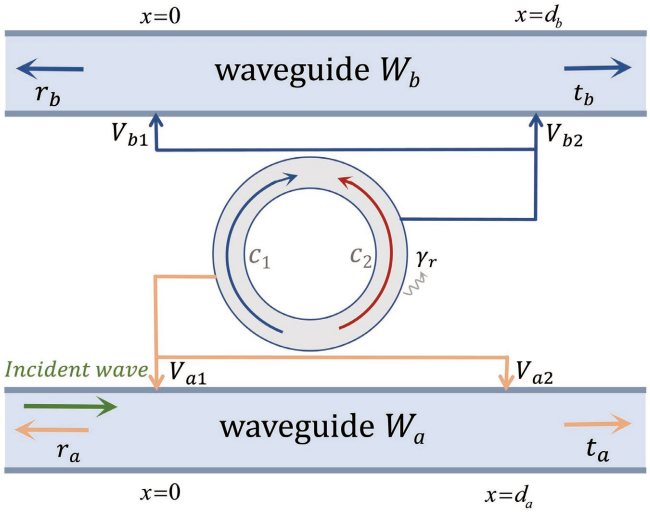

Figure 1. (Color online) Schematic diagram of single-photon routing between two waveguides. Two waveguides are simultaneously coupled to a two-mode WGM resonator via two separated coupling points located at $x=0,0$ and $x=d_a,d_b$, respectively. When a single photon is incident from the waveguide, it will be routed to four ports by the resonator.

Considering the linear dispersions of two waveguide modes and the rotating wave approximation, the real-space Hamiltonian [29] for the coupled system is given by ($\hbar=1$ hereafter)

$$\begin{aligned} H=&\sum_{s=a,b}\int \mathrm{d}x\left[-i\upsilon_g C_{Rs}^\dagger\frac{\partial}{\partial x}C_{Rs}+i\upsilon_g C_{Ls}^\dagger\frac{\partial}{\partial x}C_{Ls}\right]\\ &+\left(\omega_r-i\gamma_r\right)\left(c_1^\dagger c_1+c_2^\dagger c_2\right)+\eta\left(c_1^\dagger c_2+c_2^\dagger c_1\right)\\ &+\sum_{j=1,2}\int \mathrm{d}x\delta\left[x-\left(j-1\right)d_a\right]\left[V_{aj}\left(C_{Ra}^\dagger c_2+C_{La}^\dagger c_1\right)+H.c.\right]\\ &+\sum_{j=1,2}\int \mathrm{d}x\delta\left[x-\left(j-1\right)d_b\right]\left[V_{bj}\left(C_{Rb}^\dagger c_1+C_{Lb}^\dagger c_2\right)+H.c.\right], \end{aligned} \tag{1}$$

where υ_g is the group velocity of the moving photon, and $C_{Rs}^\dagger(x)\left[C_{Ls}^\dagger(x)\right]$ stands for the creation operator of a right(left)-propagating photon in the waveguide $W_s\left(s=a,b\right)$ at the position x. η is the inter-mode backscattering strength between two degenerate modes. The coupling strengths are generally complex coefficients, which are denoted as $V_{aj}=V_a\mathrm{e}^{i\phi_j}$ and $V_{bj}=V_b\mathrm{e}^{i\varphi_j}$ $\left(j=1,2\right)$, with the local coupling phases ϕ_j and φ_j. H.c. is the Hermitian conjugate. The interaction term in the Hamiltonian is described by direction-matching condition,

due to the fact that the light fields of the two rotating modes of the resonator come from the left and right transmission of the incident waveguide modes, and then they are transferred in the opposite directions to the drop waveguide.

Assume that a photon is input from the left side of the waveguide with the energy $E_k = \upsilon_g k = \omega$. In the single-excitation subspace the scattering eigen-state of the Hamiltonian (1) are expressed as

$$|\psi\rangle = \sum_{s=a,b} \int \mathrm{d}x \left[\Phi_{Rs}(x) C_{Rs}^{\dagger}(x) + \Phi_{Ls}(x) C_{Ls}^{\dagger}(x) \right] |\varnothing\rangle + \left(\xi_1 c_1^{\dagger} + \xi_2 c_2^{\dagger} \right) |\varnothing\rangle \tag{2}$$

where $|\varnothing\rangle$ represents the vacuum state with zero photon in the two waveguides and the resonator. ξ_1 and ξ_2 denote the excitation amplitude of two circular modes in the resonator. $\Phi_{Rs}(x)$ and $\Phi_{Ls}(x)$ describe the wave functions for the right and left guided-wave modes in two waveguides, and the corresponding expressions are

$$\begin{aligned}
\Phi_{Ra}(x) &= \mathrm{e}^{ikx} \left[\theta(-x) + t_1 \theta(x) \theta(d_a - x) + t_a \theta(x - d_a) \right], \\
\Phi_{La}(x) &= \mathrm{e}^{-ikx} \left[r_a \theta(-x) + r_1 \theta(x) \theta(d_a - x) \right], \\
\Phi_{Rb}(x) &= \mathrm{e}^{ikx} \left[t_2 \theta(x) \theta(d_b - x) + t_b \theta(x - d_b) \right], \\
\Phi_{Lb}(x) &= \mathrm{e}^{-ikx} \left[r_b \theta(-x) + r_2 \theta(x) \theta(d_b - x) \right].
\end{aligned} \tag{3}$$

Here, $\theta(x)$ is the Heaviside step function, with $\theta(0) = 1/2$. $t_{a(b)}$ and $r_{a(b)}$ describe the transmission and reflection amplitudes of single photons in four ports of two waveguides, while $t_{1(2)}$ and $r_{1(2)}$ represent the transmission and reflection amplitudes between two coupling points in two waveguides.

Solving the eigen-equation $H|\psi\rangle = E_k |\psi\rangle$, one can obtain the stationary-state expressions of the scattering coefficients as follows:

$$\begin{aligned}
t_a &= 1 - \frac{i\Gamma_a Q_2 \left[1 + \mathrm{e}^{i(\phi_a - \alpha_a)} \right] \left[1 + \mathrm{e}^{i(\alpha_a - \phi_a)} \right]}{Q_1 Q_2 - \eta^2}, \\
r_a &= -\frac{i\Gamma_a \eta \left[1 + \mathrm{e}^{i(\phi_a + \alpha_a)} \right] \left[1 + \mathrm{e}^{i(\alpha_a - \phi_a)} \right]}{Q_1 Q_2 - \eta^2}, \\
t_b &= -\frac{i\sqrt{\Gamma_a \Gamma_b} \eta \left[1 + \mathrm{e}^{i(\phi_b - \alpha_b)} \right] \left[1 + \mathrm{e}^{i(\alpha_a - \phi_a)} \right] \mathrm{e}^{i(\varphi_1 - \phi_1)}}{Q_1 Q_2 - \eta^2}, \\
r_b &= -\frac{i\sqrt{\Gamma_a \Gamma_b} Q_2 \left[1 + \mathrm{e}^{i(\phi_b + \alpha_b)} \right] \left[1 + \mathrm{e}^{i(\alpha_a - \phi_a)} \right] \mathrm{e}^{i(\varphi_1 - \phi_1)}}{Q_1 Q_2 - \eta^2},
\end{aligned} \tag{4}$$

where $\Gamma_a = V_a^2 / \upsilon_g$ and $\Gamma_b = V_b^2 / \upsilon_g$ are the effective coupling strengths between the resonator and two waveguides.

$Q_2 = \Delta\omega + i\gamma_r + i\Gamma_a \left[1 + \mathrm{e}^{i(\alpha_a + \phi_a)} \right] + i\Gamma_b \left[1 + \mathrm{e}^{i(\alpha_b - \phi_b)} \right]$ and

$Q_1 = \Delta\omega + i\gamma_r + i\Gamma_a \left[1 + \mathrm{e}^{i(\alpha_a - \phi_a)} \right] + i\Gamma_b \left[1 + \mathrm{e}^{i(\alpha_b + \phi_b)} \right]$. $\Delta\omega = \omega - \omega_r$ is the frequency detuning between the incident photon and the resonator. $\phi_a = \phi_2 - \phi_1$ and $\phi_b = \varphi_2 - \varphi_1$ are the local phase differences, and $\alpha_{a,b} = k d_{a,b}$ is the accumulated phase of the photon propagating between two coupling points, with $d_{a,b}$

being the effective propagation distance of two coupling locations due to the computation result of $\boldsymbol{k}\cdot\boldsymbol{x}$ [28].

3. Nonreciprocal Transport of Single Photons in the Coupled Single-Waveguide System

In the double-waveguide system with four output ports, the transport characteristics of the incident photons are engineered by the scattering probabilities $T_{a(b)}=\left|t_{a(b)}\right|^2$ and $R_{a(b)}=\left|r_{a(b)}\right|^2$. In this section, we investigate the nonreciprocal scattering properties of single photons in the single-waveguide structure, in which the second-point coupling $\Gamma_b=0$ is set. When a single photon is input from the right port of the bus waveguide, the propagation process is equivalent to the case that the forward photon coming from the left side of the waveguide. Therefore, applying the similar calculation methods, the backward-direction transmission amplitude t_B of the incident photon from right to left can be obtained by replacing the opposite forward-direction transmission t_F in Equation (4) with $\phi_a\to-\phi_a$. The two transmission amplitudes are expressed as $t_F=t_a$ and $t_B=1-i\Gamma_a Q_2\left[1+\mathrm{e}^{i(-\phi_a-\alpha_a)}\right]\left[1+\mathrm{e}^{i(\alpha_a+\phi_a)}\right]\Big/\left(Q_1Q_2-\eta^2\right)$, while two reflection amplitudes in the forward and backward directions are the same even exchanging the coupling phase ϕ_a.

Clearly, for the zero dissipation with $\gamma_r=0$, the single-photon transmission is reciprocal and has the same values of $T_B=\left|t_B\right|^2=T_F=\left|t_F\right|^2$. Thus, the optical nonreciprocity is caused by the difference between T_B and T_F, arising from the interference modification between backward propagation modes via the resonator dissipation, and the joint effects of two phases between two coupling points. To quantitatively describe the nonreciprocity in the system, the isolation contrast ratio is introduced as $T_I=T_B-T_F$. It is easily observed that the system displays reciprocity with $T_B=T_F$ when $T_I=0$, while perfect nonreciprocal transmission is shown for $T_B=0$, $T_F=1$ or $T_B=1$, $T_F=0$ when $T_I=\pm1$.

We first examine the influence of the phase modulation on the nonreciprocal single-photon transport properties. The transmission T_B, T_F and the contrast ratio T_I versus the detuning $\Delta\omega$ and the phases are plotted in **Figure 2**. When $\phi_a=\pi/2$ and $\alpha_a=\pi/4$ in **Figure 2(a)**, one can find that T_B and T_F display different transmission behaviors with two separate line shapes. T_F represents a Lorentzian line shape and has larger transmission probability than T_B, while the complete transmission blockading with $T_B=0$ occurs at the resonance point $\Delta\omega=0$, and the peak of T_I is less than 1 in this situation. Especially, for $\phi_a=\alpha_a=\pi/2$ in **Figure 2(b)**, the backward-direction moving photons maintain complete transmission over the entire range of the frequency detuning, as displayed by the straight red dashed lines with $T_B=1$. This can be observed from the product term of the numerator of $\left[1+\mathrm{e}^{i(\alpha_a-\phi_a)}\right]=0$ in the front formula of T_B. It means that the left-going photons propagate directly through the waveguide without absorption, since the resonator is decoupled from the waveguide, and the

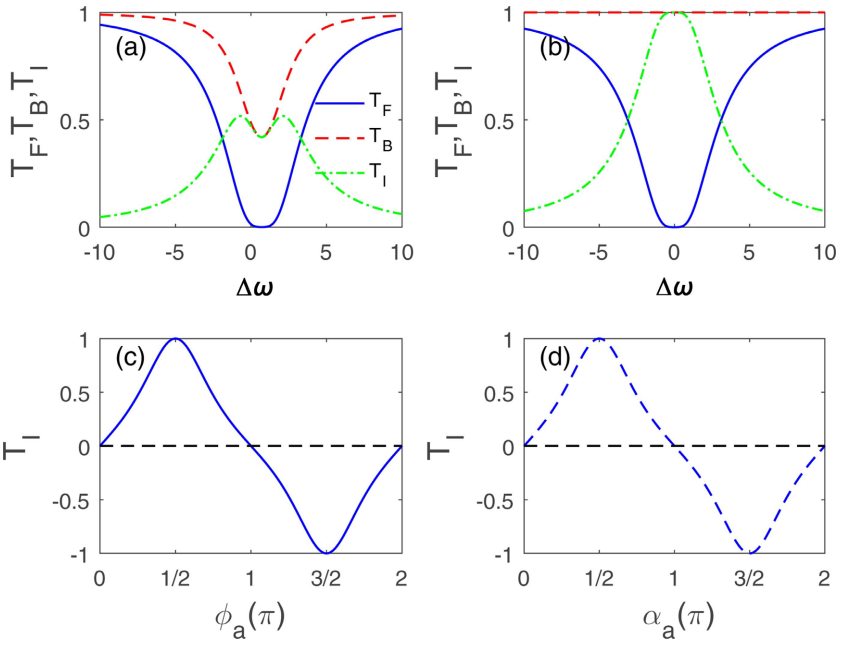

Figure 2. (Color online) Transmission T_F (solid blue curves), T_B (dashed red curves) and the contrast ratio T_I (dash-dotted green curves) versus the detuning $\Delta\omega$ for different phases in (a, b). T_I as a function of the phase ϕ_a or α_a in (c) and (d), respectively. (a) $\phi_a = \pi/4$ and $\alpha_a = \pi/2$, (b) $\phi_a = \pi/2$ and $\alpha_a = \pi/2$, (c) $\alpha_a = \pi/2$, and (d) $\phi_a = \pi/2$. Here, $\gamma_r = 2$ and $\eta = 1$ are set. All parameters except the phases are in units of Γ_a.

resonator-waveguide coupling strength becomes zero via the phase modulation. Accordingly, the right-moving photons can obtain the zero transmission of $T_F = 0$, whereas the perfect nonreciprocal transport for the contrast ratio T_I with the maximum value of 1 emerge at $\Delta\omega = 0$, arising from the constructive and destructive interferences from two phases. The contrast ratio T_I as a function of the local phase and the accumulated phase are plotted separately in **Figure 2(c)** and **Figure 2(d)**, and the two phase modulations are similar when fixing one of the two phase parameters. Note that $T_I = 1$ ($T_I = -1$) emerges corresponding to $\phi_a = \pi/2(3\pi/2)$ or $\alpha_a = \pi/2(3\pi/2)$, it implies that the symmetrical processes in two directions can be effectively regulated by the phase modulation.

In the numerical calculations, all these parameters except the phases are in units of the coupling Γ_a for simplicity. Here, γ_r, η, and Γ_a are of the same order of magnitude. These parameters are adopted to be close to the experimental results in a coupled waveguide-resonator system [30], where they are around the same order of magnitude, such as $\Gamma_a/2\pi = 6.9$ MHz, $\eta/2\pi = 5.5$ MHz, and $\gamma_r/2\pi = 2.5$ MHz. Although $\omega_r = 5.94$ GHz is large and not on the same order of magnitude of MHz, we focus on the detuning $\Delta\omega = \omega - \omega_r$ between the incident photon frequency and the resonator's intrinsic frequency.

To get a deeper insight into the control of the nonreciprocal behaviors via the phases, **Figure 3** displays these transmission varying with the phase parameters.

By comparing Figure 3(a) and Figure 3(b), one can find from the inverse peak and dip locations that the two transmission probabilities T_B and T_F have opposite responses for the local phase difference ϕ_a. For example, for the fixed phase of $\alpha_a = \pi/2$, $T_F = 1$ and $T_B = 0$ for $\phi_a = 3\pi/2$, while $T_F = 0$ and $T_B = 1$ for $\phi_a = \pi/2$. Figure 3(c) represents the contrast ratio of the transmission probabilities for the left-going and right-going photons. As expected, two optimal nonreciprocal transmission windows are presented in two similar bright red or blue regions. The maximum $T_I = \pm 1$ is obtained by adjusting ϕ_a to be $\pi/2$ and $3\pi/2$, respectively. Symmetrically, similar conclusions can be drawn for the accumulated phase α_a. Figure 3(d) shows that four symmetric dark-red elliptical region with high-value ratio of T_I appears in the (α, ϕ) plane, and two peaks and two dips in the centers of the four areas indicate that perfect single-photon nonreciprocal transmission of $T_I = \pm 1$ can be achieved only when the phases meet the condition of $\alpha_a = (\pi/2, 3\pi/2)$ and $\phi_a = (\pi/2, 3\pi/2)$.

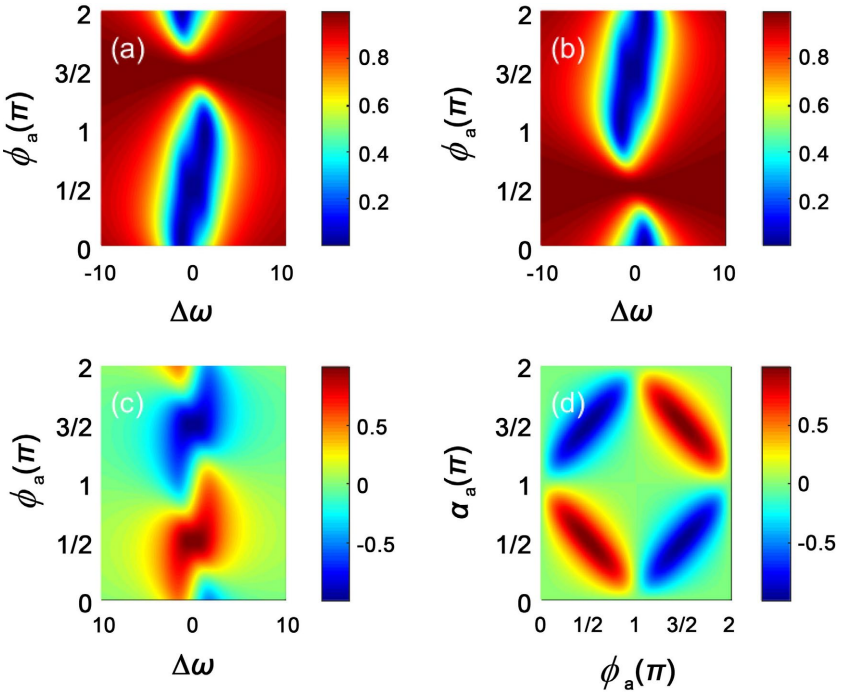

Figure 3. (Color online) Transmission T_F, T_B and the contrast ratio T_I as a function of ϕ_a and $\Delta\omega$ in (a), (b) and (c), respectively. T_I as a function of ϕ_a and α_a in (d). $\alpha_a = \pi/2$ in (a, b, c). Other parameters are same as that in Figure 2.

Note that the resonator dissipation is also a crucial parameter to function the system nonreciprocity. Further, the influence of the dissipation γ_r and the intermode backscattering strength η on the nonreciprocal transmission T_I is also researched. When $\alpha_a = \phi_a = \pi/2$ is fixed, these parameters to obtain the maximum value of $T_I = 1$ are governed by the equation of $\gamma_r^2 - 2\gamma_r + \eta^2 - \Delta\omega^2 = 0$ or $\Delta\omega(\gamma_r - 1) = 0$, which is reduced by $T_F = 0$. As shown in Figure 4(a), at the resonance point $\Delta\omega = 0$, a dark-red narrow arc-shaped region emerges in the

(η, γ_r) plane, which means that the maximum T_I can be achieved via multiple parameter values, since there is a series of solutions related to dissipation and backscattering strength for the result of $\gamma_r = 1 \pm \sqrt{1-\eta^2}$. However, for the non-zero detuning, $\gamma_r = 1$ is determined, and thus η can get a single definite solution $\eta = \sqrt{1+\Delta\omega^2}$, which is related to the detuning. As an example, Figure 4(b) displays a maximum peak with $(\eta, \gamma_r) = (3.16, 1)$ located at the center of the dull-red circular region, when $\Delta\omega = 3$ is set. Therefore, over a wide frequency range, perfect nonreciprocity can be regulated by tuning the dissipation and the inter-mode backscattering strength.

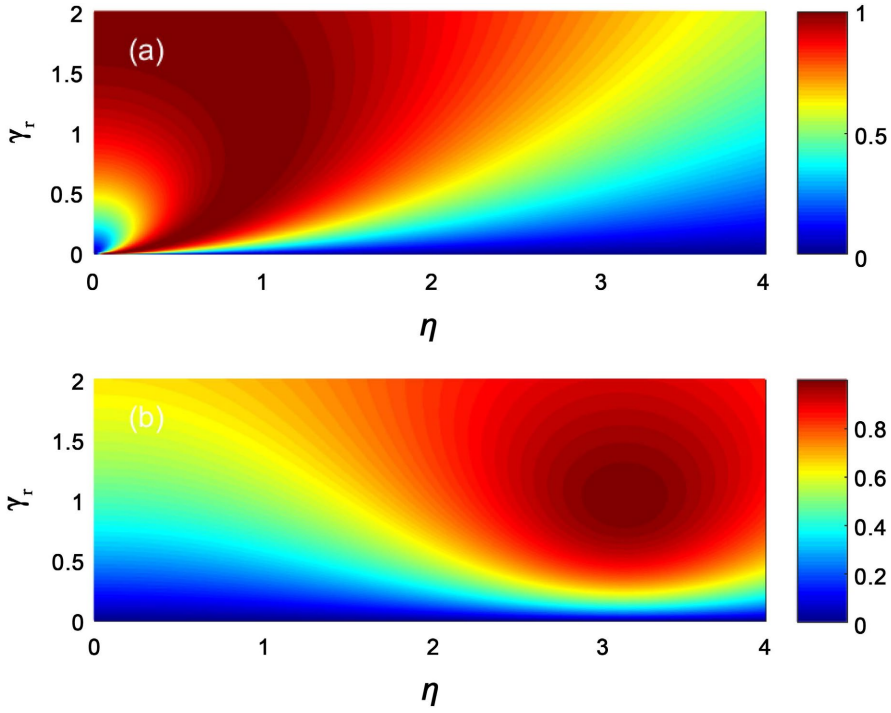

Figure 4. (Color online) T_I as a function of η and γ_r for different detunings: (a) $\Delta\omega = 0$ and (b) $\Delta\omega = 3$. Other parameters are same as that in Figure 2(b).

4. Directional Single-Photon Routing in the Coupled Two-Waveguide System

As a comparison with the photon transport in the single-waveguide case, quantum routing of single photons in the coupled double-waveguide waveguide is also examined. When a photon enters into the bus waveguide, it will be scattered by the resonator, and the photon probability flow will be distributed at four ports. Note that the total sum of the photon flow will remain unchanged (see the green straight line), when the dissipations are not taken into account, since the conservation relation $T_m + R_m + T_n + R_n = 1$ holds on. Note that the sum of the photon flow will remain unchanged in the absence of the resonator dissipation, because the conservation relation $T_a + R_a + T_b + R_b = 1$ holds, as shown by the green straight lines in Figure 5(a) and Figure 5(b). For simplicity, $\gamma_r = 0$ and $\Gamma_b = \Gamma_a$

are assumed in the numerical calculations. Then, we consider how these parameters affect the routing features transferring between two different waveguide channels, and thus we focus on the routing efficiency from the bus waveguide to another. For comparison, we first consider the single-point coupling in the coupled system for the straight waveguides, corresponding to $V_{a2} = V_{b2} = 0$. In this case, the routing amplitudes in Equation (4) can be simplified as

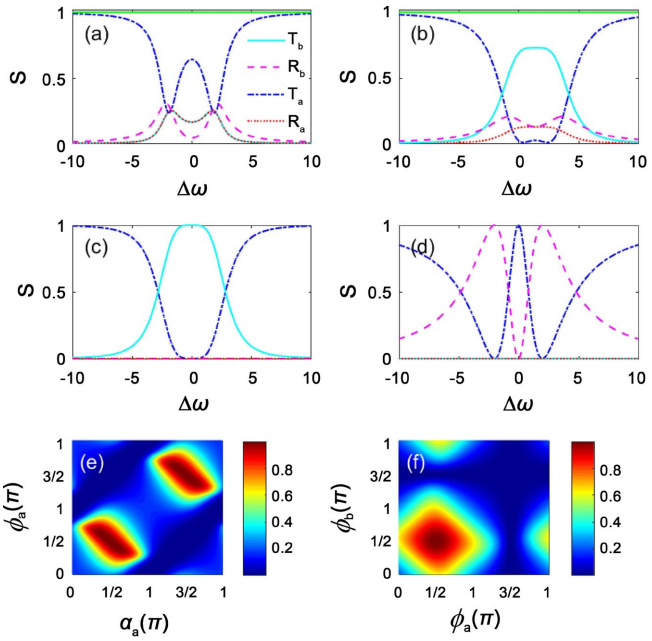

Figure 5. (Color online) Four-port routing S (T_a for dash dotted blue curves, R_a for dotted red curves, T_b for solid cyan curves, and R_b for dashed pink curves) versus the frequency detuning $\Delta\omega$. (a) the single-point coupling case independent of the phases, (b) $\phi_a = \phi_b = \pi/4$, (c) $\phi_a = \phi_b = \pi/2$, and (d) $\phi_a = \pi/2$, $\phi_b = 3\pi/2$. $T_b = R_a$ in (a), $R_b = R_a = 0$ in (c), and $T_b = R_a = 0$ in (d). These curves corresponding to equal transmission overlap completely in the scattering spectra. The green straight line denotes the total sum of the photon flow. T_b as a function of α_a and ϕ_a in (e), and R_b as a function of ϕ_a and ϕ_b in (f). $\phi_a = \phi_b$ and $\alpha_a = \alpha_b$ are set in (e), while only $\alpha_a = \alpha_b$ is taken in (f). These parameters are $\Gamma_b = 1$, $\gamma_r = 0$, $\eta = 2$, and $\alpha_a = \alpha_b = \pi/2$.

$$
\begin{aligned}
t_a &= 1 - \frac{i\Gamma_a Q_2}{Q^2 - \eta^2}, \\
r_a &= -\frac{i\Gamma_a \eta}{Q^2 - \eta^2}, \\
t_b &= -\frac{i\sqrt{\Gamma_a \Gamma_b}\,\eta e^{i(\varphi_1 - \phi_1)}}{Q^2 - \eta^2}, \\
r_b &= -\frac{i\sqrt{\Gamma_a \Gamma_b}\, Q_2 e^{i(\varphi_1 - \phi_1)}}{Q^2 - \eta^2},
\end{aligned}
\tag{5}
$$

with $Q = \Delta\omega + i\gamma_r + i\Gamma_a/2 + i\Gamma_b/2$. It is evident that these scattering probabilities are strongly independent of the phases. Due to the direction-matching effect, the

scattering of incident light through the symmetrical coupling channels of $\Gamma_b = \Gamma_a$ into two left and right ports in the two waveguides leads to the same probability, *i.e.*, $T_b = R_a$. The routing spectra of these two ports overlap as shown in Figure 5(a), and they have the equal maximum peak values of 0.25. Correspondingly, another port routing R_b scattered by the resonator is bigger than T_b, but the routing efficiency is still low with less than 0.5.

While for the two-point coupling case of the resonator and the waveguides, routing efficiency is improved by the phase modulation. Figure 5(b) shows that the routing efficiency of T_b increases compared to the single-point coupling case when $\phi_a = \phi_b = \pi/4$ and $\alpha_a = \alpha_b = \pi/2$. Specially, when $\phi_a = \phi_b = \pi/2$ and $\gamma_r = 0$ in Figure 5(c), the routing efficiency of T_b can reach the maximum value of unity at the resonance point $\Delta\omega = 0$ via the asymmetrical waveguide-resonator coupling, meanwhile the two left routing ports are decoupled from waveguides with the zero couplings, which means the transfer to the two ports are blocked, and $R_b = R_a = 0$ for all frequencies. Therefore, the directional routing to the right port of the waveguide W_b can be implemented by modulating the phases, under the phase-dependent interference effects. Similarly, the directional routing to the left port of the waveguide W_b can be also performed by modulating the phase as $\phi_a = \pi/2$ and $\phi_b = 3\pi/2$. In the case $T_b = R_a = 0$ for all frequencies, and two peaks with 100% routing probability emerge in Figure 5(d). These results clearly show that the proposed routing scheme can transfer photons from the input port to another arbitrarily selected port in the drop waveguide with a perfect routing through the appropriate phase modulation. Moreover, Figure 5(e) and Figure 5(f) display the dependence of the routing efficiency of T_b on the phases, respectively. It is observed that for $\alpha_a = \alpha_b = \pi/2$, the maximum value of targeted single-photon router with 100% routing probability T_b emerges at $\phi_a = \phi_b = \pi/2$ or $\phi_a = \phi_b = 3\pi/2$, while the maximum value of R_n appears only when the phases meet the condition of $\phi_a = \pi/2$ and $\phi_b = 3\pi/2$ when $\alpha_a = \alpha_b = \pi/2$ is fixed.

It is worth noting that inter-mode backscattering strength η also plays a significant role in achieving directional routing. As seen from Figure 6(a), for $\eta = 1$, two peaks for R_b with the maximum routing probability of unity are presented, while a single peak for T_b with the peak value less than unity appears at the resonance point. Increasing η from 1 to 3, two peaks for T_b emerge, which indicates that the the maximum routing probability of T_b is sensitive to η. Figure 6(b) also shows the continuous variation trend of two routing maximum in a wide frequency range for the varying η. It shows that the maximum routing probability $R_b^m = 1$ independent of η arises, while there is the maximum routing probability $T_b^m = 1$ when η exceeds 2. For comparison, Figure 6(c) and Figure 6(d) also display separately the dependence of the routing probability of T_b and R_b on η. It can be found that two similar V-shaped regions denoting high routing efficiency appear in two planes, but both have significantly different base positions of 0 and 2. Through the analysis of Equation (4), the maximum transfer rate

$T_b = 1$ can be realized when satisfying the condition $\Delta\omega = \pm\sqrt{\eta^2 - 4}$. Mathematically $\eta \geq 2$ is required to get the two real number solutions.

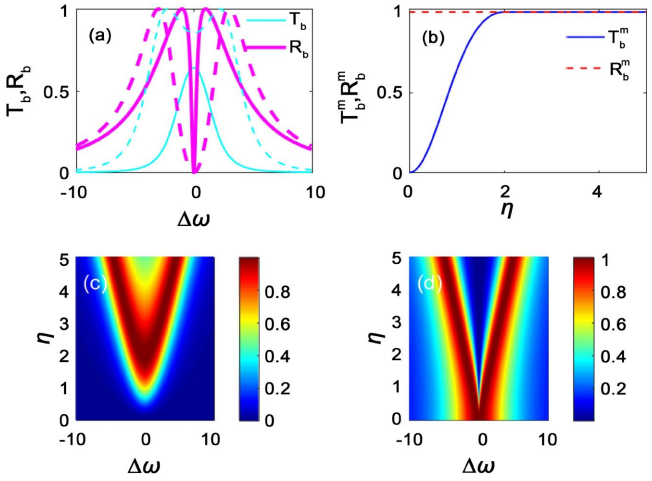

Figure 6. (Color online) (a) Routig efficiency T_b (thin curves) and R_b (thick curves) as a function of the detuning $\Delta\omega$ for different backscattering strengths: $\eta = 1$ (solid lines) and $\eta = 3$ (dashed lines). (b) The maximum routing peak T_b^m (solid blue line) and R_b^m (dashed red curve) in the frequency range versus η. (c) T_b and (d) R_b as a function of η and $\Delta\omega$. $\Gamma_b = 1$, $\gamma_r = 0$, and $\alpha_a = \alpha_b = \phi_a = \pi/2$. $\phi_b = \pi/2$ for T_b and $\phi_b = 3\pi/2$ for R_b.

Physically, the scenario results from the mode direction-matching transmission. The routing photon into the left port of waveguide W_b is redirected by the counter-clockwise mode for the directly incident photon, and the routing efficiency can reach 1 at some frequencies for these straight-through photons. However, the routing photon into the right port of waveguide W_b originates from the photon transmitted along the clockwise mode, which is coupled through backscattering. When the backscattering strength is weak, not all photons can be transferred to the right port, and thus the routing efficiency can not reach 1. When increasing the backscattering strength, more photons enter this channel, thereby reaching the maximum efficiency value of 1. Experimentally, the resonator-waveguide coupling strength presented by the phases can be tuned by the their separation and mode polarization direction. The backscattering strength is adjustable via a single subwavelength scatterer, which is attached on the resonator surface and results in a modification of the mode density by varying the Rayleigh scattering rate [31].

The effects of some other parameters on the quantum routing are remarked in **Figure 7**. When the different couplings are taken into accounted, it can be found in **Figure 7(a)** that the maximum routing efficiency emerges for the equal coupling $\Gamma_b/\Gamma_a = 1$. **Figure 7(b)** further shows that the maximum value in the wide frequency scope occurs at the equal coupling, since the complete photon transfer between two waveguides appears only over the identical coupling channels. When the inevitable dissipation is considered in **Figure 7(c)**, the routing peaks decrease

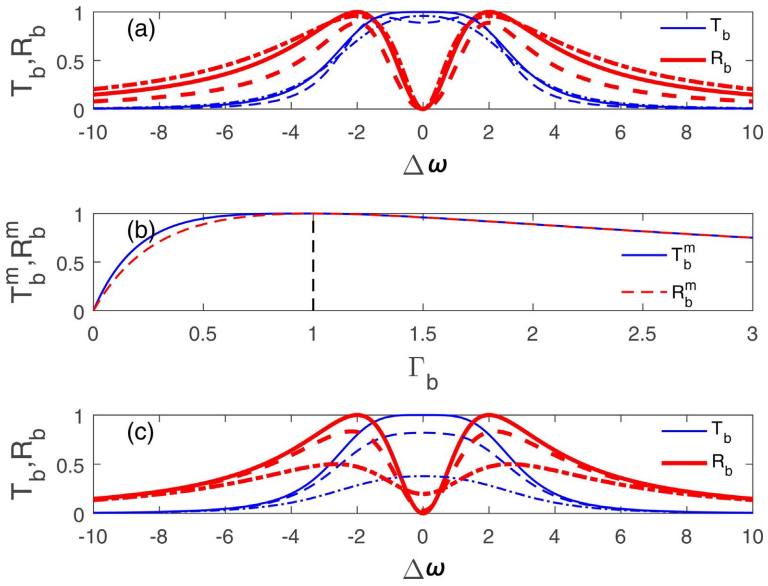

Figure 7. (Color online) T_b (thin curves) and R_b (thick curves) as a function of the detuning $\Delta\omega$ for different parameters. (a) $\Gamma_b = 0.5$ (solid lines), $\Gamma_b = 1$ (dashed lines), and $\Gamma_b = 1.5$ (dash dotted lines). (c) $\gamma_r = 0$ (solid lines), $\gamma_r = 0.2$ (dashed lines), and $\gamma_r = 1$ (dash dotted lines). The maximum routing peak T_b^m (solid blue line) and R_b^m (dashed red curve) in the frequency range versus Γ_b in (b). Other parameters are the same as that in **Figure 5(c)**.

with the increase of dissipation due to the photon leakage of the resonator. However, high routing efficiency is available for the general loss, such as $T_b = 0.83$ at $\gamma = 0.2$.

5. Conclusion

In summary, we have examined the tunable single-photon nonreciprocal transmission and directional routing in a microresonator-waveguide structure with multiple coupling points. Applying a full quantum approach related to the real-space Hamiltonian, the routing probabilities of single photons from the incident waveguide to another are obtained exactly. Our results show that the perfectly nonreciprocal transmission of single photons can be manipulated by the combinational effect of the local coupling phase and the accumulated phase between two coupling points of the resonator and the bent waveguides. Similarly, the high-efficiency targeted quantum routing in two ports of the drop waveguide can be performed by varying the related phases of the resonator due to the phase-dependent interference effect. The optimal parameter sets of the perfectly nonreciprocal transmission and the directional routing with the unity probability in the ideal case are presented as $(\alpha_a = \alpha_b = \phi_a, \phi_b, \eta, \gamma) = (\pi/2, \pi/2, 2, 2)$ and $(\alpha_a = \alpha_b = \phi_a, \phi_b, \eta, \gamma) = [\pi/2, \pi/2(3\pi/2), 2, 0]$, respectively. Of course, the bending loss or manufacturing tolerance in the coupling distance and the approximate linear dispersion are ignored for simplicity, which indeed reduces faintly the scattering performance of the system. These results are expected to provide potential

applications in quantum photonic circuits, integrated optical chips and quantum information processing.

Funding

This work was supported by Key Laboratory of Low Dimensional Quantum Materials and Sensor Devices of Jiangxi Education Institutes (No. GanJiaoKeZi-20241301), and Jiangxi Provincial Natural Science Foundation (Grant No. 20212BAB201014).

Conflicts of Interest

The authors declare no conflicts of interest regarding the publication of this paper.

References

[1] Ladd, T.D., Jelezko, F., Laflamme, R., Nakamura, Y., Monroe, C. and O'Brien, J.L. (2010) Quantum Computers. *Nature*, **464**, 45-53. https://doi.org/10.1038/nature08812

[2] Gisin, N. and Thew, R. (2007) Quantum Communication. *Nature Photonics*, **1**, 165-171. https://doi.org/10.1038/nphoton.2007.22

[3] Kimble, H.J. (2008) The Quantum Internet. *Nature*, **453**, 1023-1030. https://doi.org/10.1038/nature07127

[4] Goban, A., Hung, C., Yu, S., Hood, J.D., Muniz, J.A., Lee, J.H., *et al.* (2014) Atom-Light Interactions in Photonic Crystals. *Nature Communications*, **5**, Article No. 3808. https://doi.org/10.1038/ncomms4808

[5] Roy, D., Wilson, C.M. and Firstenberg, O. (2017) Colloquium: Strongly Interacting Photons in One-Dimensional Continuum. *Reviews of Modern Physics*, **89**, Article ID: 021001. https://doi.org/10.1103/revmodphys.89.021001

[6] Wang, D., Zhou, H., Guo, M., Zhang, J., Evers, J. and Zhu, S. (2013) Optical Diode Made from a Moving Photonic Crystal. *Physical Review Letters*, **110**, Article ID: 093901. https://doi.org/10.1103/physrevlett.110.093901

[7] Wu, J., Artoni, M. and La Rocca, G.C. (2014) Non-Hermitian Degeneracies and Unidirectional Reflectionless Atomic Lattices. *Physical Review Letters*, **113**, Article ID: 123004. https://doi.org/10.1103/physrevlett.113.123004

[8] Zheng, A., Zhang, G., Chen, H., Mei, T. and Liu, J. (2017) Nonreciprocal Light Propagation in Coupled Microcavities System Beyond Weak-Excitation Approximation. *Scientific Reports*, **7**, Article No. 14001. https://doi.org/10.1038/s41598-017-14397-7

[9] Xia, X., Zhang, X., Xu, J., Li, H. and Yang, Y. (2024) Optical Nonreciprocity in an Asymmetric Cavity Containing Two Asymmetrically Arranged Atoms. *Physical Review A*, **109**, Article ID: 053709. https://doi.org/10.1103/physreva.109.053709

[10] Hafezi, M. and Rabl, P. (2012) Optomechanically Induced Non-Reciprocity in Microring Resonators. *Optics Express*, **20**, 7672-7684. https://doi.org/10.1364/oe.20.007672

[11] Dong, Y., Huang, X. and Zhang, G. (2026) Nonreciprocity of Intense Light Field and Weak Quantum Signal in Optomechanical Systems with Three-Mode Parametric Interactions. *Physical Review A*, **113**, Article ID: 013513. https://doi.org/10.1103/8kg8-brsx

[12] Shen, Z., Zhang, Y., Chen, Y., Zou, C., Xiao, Y., Zou, X., *et al.* (2016) Experimental Realization of Optomechanically Induced Non-Reciprocity. *Nature Photonics*, **10**, 657-661. https://doi.org/10.1038/nphoton.2016.161

[13] Yan, W., Ni, W., Zhang, J., Zhang, F. and Fan, H. (2018) Tunable Single-Photon Diode by Chiral Quantum Physics. *Physical Review A*, **98**, Article ID: 043852. https://doi.org/10.1103/physreva.98.043852

[14] Xia, K., Nori, F. and Xiao, M. (2018) Cavity-Free Optical Isolators and Circulators Using a Chiral Cross-Kerr Nonlinearity. *Physical Review Letters*, **121**, Article ID: 203602. https://doi.org/10.1103/physrevlett.121.203602

[15] Poudyal, B. and Mirza, I.M. (2020) Collective Photon Routing Improvement in a Dissipative Quantum Emitter Chain Strongly Coupled to a Chiral Waveguide QED Ladder. *Physical Review Research*, **2**, Article ID: 043048. https://doi.org/10.1103/physrevresearch.2.043048

[16] Ko, M., Kim, N., Choe, H., Ri, S., Ryom, J., Ri, C., *et al.* (2019) Feasible Surface Plasmon Routing Based on the Self-Assembled InGaAs/GaAs Semiconductor Quantum Dot Located between Two Silver Metallic Waveguides. *Plasmonics*, **15**, 271-277. https://doi.org/10.1007/s11468-019-01022-8

[17] Huang, J., Wang, J., Li, Y., Wang, Y. and Huang, Y. (2019) Tunable Quantum Routing via Asymmetric Intercavity Couplings. *Quantum Information Processing*, **18**, Article No. 59. https://doi.org/10.1007/s11128-019-2176-y

[18] Huang, J., Feng, X., Xu, Z., Li, Y. and Wu, K. (2023) Tunable Bandpass Routers of Single Photons with Three-Level Emitters. *Quantum Information Processing*, **22**, Article No. 285. https://doi.org/10.1007/s11128-023-04039-5

[19] Wu, J., Dong, J., Xu, Y., Zou, B. and Zhang, Y. (2022) Multichannel Adjustable Single-Photon Router Based on Large Detuning. *Physical Review Applied*, **18**, Article ID: 054007. https://doi.org/10.1103/physrevapplied.18.054007

[20] Ryom, J., Ri, G., Kim, N., Ko, M., Choe, I. and Ri, S. (2023) Entanglement Generated in Quantum Dot-Cavity Coupled System Mediated by Plasmonic Waveguide. *Journal of Low Temperature Physics*, **213**, 80-91. https://doi.org/10.1007/s10909-023-02982-2

[21] Saha, U., Siverns, J.D., Hannegan, J., Prabhu, M., Quraishi, Q., Englund, D., *et al.* (2023) Routing Single Photons from a Trapped Ion Using a Photonic Integrated Circuit. *Physical Review Applied*, **19**, Article ID: 034001. https://doi.org/10.1103/physrevapplied.19.034001

[22] Chen, W., Zhang, J., Peng, B., Özdemir, Ş.K., Fan, X. and Yang, L. (2018) Parity-time-symmetric Whispering-Gallery Mode Nanoparticle Sensor [Invited]. *Photonics Research*, **6**, A23. https://doi.org/10.1364/prj.6.000a23

[23] Aoki, T., Parkins, A.S., Alton, D.J., Regal, C.A., Dayan, B., Ostby, E., *et al.* (2009) Efficient Routing of Single Photons by One Atom and a Microtoroidal Cavity. *Physical Review Letters*, **102**, Article ID: 083601. https://doi.org/10.1103/physrevlett.102.083601

[24] O'Shea, D., Junge, C., Volz, J. and Rauschenbeutel, A. (2013) Fiber-Optical Switch Controlled by a Single Atom. *Physical Review Letters*, **111**, Article ID: 193601. https://doi.org/10.1103/physrevlett.111.193601

[25] Cao, C., Duan, Y., Chen, X., Zhang, R., Wang, T. and Wang, C. (2017) Implementation of Single-Photon Quantum Routing and Decoupling Using a Nitrogen-Vacancy Center and a Whispering-Gallery-Mode Resonator-Waveguide System. *Optics Express*, **25**, 16931-16946. https://doi.org/10.1364/oe.25.016931

[26] Bi, L., Hu, J., Jiang, P., Kim, D.H., Dionne, G.F., Kimerling, L.C., *et al.* (2011) On-chip Optical Isolation in Monolithically Integrated Non-Reciprocal Optical Resonators. *Nature Photonics*, **5**, 758-762. https://doi.org/10.1038/nphoton.2011.270

[27] Lenferink, E.J., Wei, G. and Stern, N.P. (2014) Coherent Optical Non-Reciprocity in Axisymmetric Resonators. *Optics Express*, **22**, 16099-16111. https://doi.org/10.1364/oe.22.016099

[28] Liu, W., Lin, Y., Li, J. and Wang, X. (2022) Nonreciprocal Waveguide-QED for Spinning Cavities with Multiple Coupling Points. *Frontiers in Physics*, **10**, Article 894115. https://doi.org/10.3389/fphy.2022.894115

[29] Shen, J. and Fan, S. (2009) Theory of Single-Photon Transport in a Single-Mode Waveguide. II. Coupling to a Whispering-Gallery Resonator Containing a Two-Level Atom. *Physical Review A*, **79**, Article ID: 023838. https://doi.org/10.1103/physreva.79.023838

[30] Aoki, T., Dayan, B., Wilcut, E., Bowen, W.P., Parkins, A.S., Kippenberg, T.J., *et al.* (2006) Observation of Strong Coupling between One Atom and a Monolithic Microresonator. *Nature*, **443**, 671-674. https://doi.org/10.1038/nature05147

[31] Srinivasan, K. and Painter, O. (2007) Mode Coupling and Cavity-Quantum-Dot Interactions in a Fiber-Coupled Microdisk Cavity. *Physical Review A*, **75**, Article ID: 023814. https://doi.org/10.1103/physreva.75.023814